Exploring solutions for Type-II superconductors in critical state

C. Romero-Salazar and O.A. Hernández-Flores
Escuela de Ciencias, Universidad Autónoma Benito Juárez de Oaxaca,
Av. Universidad s/n. Colonia Cinco Señores, Oaxaca de Juárez, 68120, Oax, México,
e-mail: cromeros@sirio.ifuap.buap.mx; omar22121972@yahoo.com.mx

Received 13 June 2012; accepted 28 November 2012

An analytical solution is found for magnetic induction in a type-II superconducting plate in parallel geometry. In this study, critical current density is modeled following the Ming Xu *et al.,* approach which requires the adjusting parameters n and B^*. A symmetry relation between the generating equations of the $H > 0$ and $H < 0$ cases is presented, as well as an equivalence between vertical and power laws for a superconductor in steady state. We present a systematic procedure for identifying magnetic induction profiles and we analyze the physical characteristics of the superconducting plate when n and B^* vary. Specifically, we present flat surface plots of the penetration field, double penetration field, critical current density and, finally, an application of our results to calculate the shielding field, which prevents the occurrence flux jumps.

Keywords: Type-II superconductors; critical state; stationary state.

PACS: 74.20.-z; 74.25.Ha; 74.25.Wx; 74.25.Sv

1. Introduction

Over the last forty years, it has been well established that the macroscopical magnetic response of irreversible type-II superconductors is controlled by two fundamental processes: the *flux pinning* due to vortices with deffects or inhomogeneities interactions and the *flux-line cutting* due to adjacent plane vortex interactions. The latter occurs when the applied magnetic field contains several components or variable orientation. Both phenomena have been studied employing models based on Bean theory [1]: The Double Generalized Critical-State model [2,3], the Two-Velocity Hydrodynamic model [5,6], the Optimal Control model [4], the Elliptic Flux-Line-Cutting Critical-State model [7], and, most recently, the Elliptic-Extended Flux-Line-Cutting Critical-State model [8]. These models employ a material equation based on the fact that an electric field $\mathbf{E}$ can exist inside a sample in the superconducting state, and the magnitude of the supercurrent density $\mathbf{J}$ can possess a finite critical value J_c, that persists even in absense of $\mathbf{E}$.

Bean proposed that a superconductor can hold a limited superconducting current density $J_c(B)$ and analyzed its magnetic properties by solving Ampéres law,

$$\nabla \times \mathbf{H} = \pm \mathbf{J}, \tag{1}$$

where $|\mathbf{J}| = J_c$. Any electromotive force greater than this value will cause the supercurrent to flow locally and the material enter a resistive state.

It is of interest to study the electromagnetic properties of type-II superconductors subjected to slowly increased external magnetic fields $\mathbf{H}$. Flux distribution can fall into a variety of metaestable states, which change only when the magnitude of the local current density $\mathbf{J}$ exceeds the critical current density $J_c = J_c(B)$. The material can relax through a succession of steady or quasi-steady states, even though flux transport occurs in the interior due to vortex bundling induced by the Lorentz force $\mathbf{F}_L = \mathbf{J} \times \mathbf{B}$, once the pinning force $\mathbf{F}_p$ is overcome.

From current-voltage curves analysis, is well known that changes in magnetic flux inside the superconductor will generate an electric field. Flux movement resists through a friction force due to pinning centers, together with a viscous force, although the latter is usually less than the former. If J_c is exceeded during transport measurements an electric field $\mathbf{E}$ is detected due to the presence of electrostatic charges at the terminals array. On the other hand, if there is a flux leak in a superconducting ring, $\mathbf{E}$ is induced due to the abscence of electrostatic charge, even if local conditions are identical to those in the transport measurement case.

In the present study, we perform a theoretical study of the macroscopic properties of type-II superconducting plates in parallel geometry.

As the external magnetic field varies in magnitude but not in direction, it is possible to find analytical solutions if we consider an infinite sample with finite thickness. We analyze the stationary state of two standard material relations $E(J)$.

To the best of the authors' knowledge, a detailed presentation of how magnetic induction profiles can be obtained has not yet been carried out. Experimental and theoretical studies have focused on magnetization and hysteresis curves calculation [9,11], as well as numerical calculations of the magnetic induction profiles of HTSC [12]. In the present work, we employ the Kim-generalized function for the critical current density $J_c(B)$ to perform both a systematic presentation for identifying magnetic induction profiles and a detailed analysis of how the superconducting behavior depends on the parametricality of n and B^*.

2. Steady-State Solutions and the E − J relationship

The Maxwell equations in a medium are:

$$\nabla \times \mathbf{H} = \mathbf{J} + \partial_t \mathbf{D} \tag{2}$$

$$\nabla \times \mathbf{E} = -\partial_t \mathbf{B} \tag{3}$$

$$\nabla \cdot \mathbf{D} = \rho \tag{4}$$

$$\nabla \cdot \mathbf{B} = 0. \tag{5}$$

The request for additional equations is well known. These so-called constitutive relations, for an anisotropic medium, can be written as follows:

$$\begin{aligned} \mathbf{J} &= \overleftrightarrow{\sigma} \cdot \mathbf{E} \\ \mathbf{D} &= \overleftrightarrow{\epsilon} \cdot \mathbf{E} \\ \mathbf{B} &= \overleftrightarrow{\mu} \cdot \mathbf{H} \end{aligned} \tag{6}$$

where the conductivity $\overleftrightarrow{\sigma}$, permittivity $\overleftrightarrow{\epsilon}$, and permeability $\overleftrightarrow{\mu}$, are second rank tensors. In our theoretical study, the superconductor is isotropic; the net electrostatic charge distribution is null; temporal variations of the electrical displacement are negligible, and for the sake of simplicity we assume, with good approximation, the boundary condition $\mathbf{B} \approx \mu_0 \mathbf{H}$.

We employ the Bean current-electric field relationship:

$$\mathbf{J} = J_c(B)\frac{\mathbf{E}}{E}. \tag{7}$$

This multicomponent model considers that $\mathbf{E} \| \mathbf{J}$ and does not include flux-line cutting effects. To obtain the $\mathbf{J}$ and $\mathbf{B}$ profiles and the magnetization of a superconductor in a steady state, one of two procedures is generally followed: an analytic one, solving the Ampéres (1) and materials law (7) system of equations, applying the condition $\partial_t B = 0$, or a numeric one [3,12], solving the Ampéres (1), Faradays (3) and (7) system of equations. In the latter, both slow variations of the surface boundary conditions and small electric fields are considered; thus the resulting $\mathbf{B}$ and $\mathbf{J}$ profiles are considered quasi-relaxed. In this work we choose a third option: a combination of the two mentioned above, which will be detailed below.

Our system is an infinite superconducting plate of thickness D, a scheme is shown in Fig. 1. It is subjected to a magnetic field $\mathbf{H} = H\mathbf{e}_z$, surface barriers against flux entrance or exit are negligible, and $H_{c1} \ll H_{c2}$. Once $\mathbf{H}$ has penetrated the sample, a superconducting current density $\mathbf{J} = J\mathbf{e}_y$ appears. If there is no remanent field and $\mathbf{H} > 0$, the current flows counterclockwise; if $\mathbf{H} < 0$, it flows clockwise.

Since the magnetic induction $\mathbf{B} = B\mathbf{e}_z$ only has an $x-$component, using Ampéres law, we obtain $\partial_x B = -\mu_0 J_y$. Furthermore, since $\mathbf{E} \| \mathbf{J}$, then $\mathbf{E} = |\mathbf{E}|\mathbf{e}_J = E(J)\mathbf{e}_y$, where $\mathbf{e}_J = \mathbf{J}/J$ is a unit vector. Therefore, Faradays law is written as $\partial_t B = -\partial_x E(J(x))$.

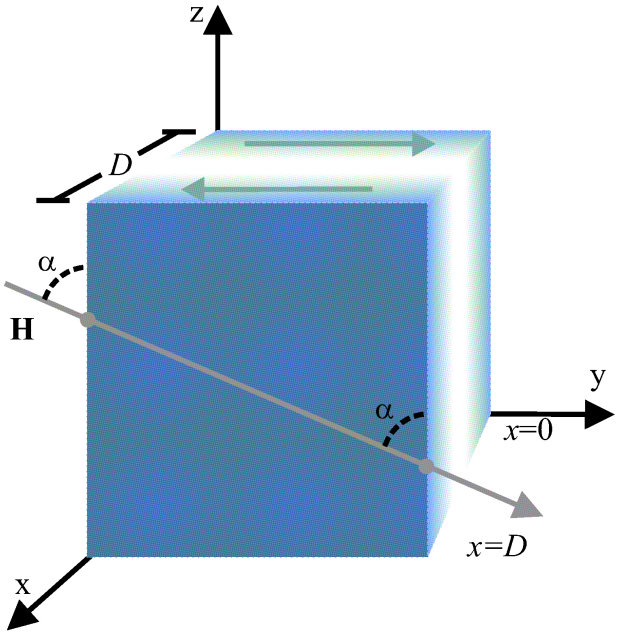

FIGURE 1. Scheme of a portion of an infinite type-II superconducting plate of thickness D.

Here, we use the vertical law to model $E(J)$:

$$E(J) = \begin{cases} 0 & |J| \le J_c, \\ \rho(J - \text{signo}(J)J_c) & |J| \ge J_c. \end{cases} \tag{8}$$

where

$$\text{signo}(J) = \begin{cases} +1 & H > 0, \quad x \in [0, D/2] \\ -1 & H > 0, \quad x \in [D/2, D] \\ -1 & H < 0, \quad x \in [0, D/2] \\ +1 & H < 0, \quad x \in [D/2, D] \end{cases} \tag{9}$$

Substituting the latter in Faradays law yields:

$$\partial_t B = -\partial_x\{\rho(J - \text{signo}(J)J_c)\},$$

subsequently, substituting Ampéres law in the previous equation, we found:

$$\partial_t B = -\partial_x \left\{ \rho \left(-\frac{1}{\mu_0}\partial_x B - \text{signo}(J)J_c \right) \right\}.$$

Since the focus of our study is steady-state solutions, we establish the condition $\partial_t B = 0$. This restriction reduces the problem to solving a first-order non-linear ordinary differential equation:

$$\frac{dB}{dx} + \text{signo}(J)\mu_0 J_c = -\frac{\mu_0 C'}{\rho} \tag{10}$$

We employ the empirical Kim-Anderson generalized law for current-field relationship proposed by Xu *et al.*, [13]:

$$J_c = \frac{J_{c0}}{\left(1 + \frac{B}{B^*}\right)^n} \tag{11}$$

where J_{c0} is the maximum value of the critical current density given by the formula:

$$J_c(0) = \left[\left(1+\frac{B_p}{B^*}\right)^{n+1} - 1\right]\frac{2B^*}{(n+1)\mu_0 d}, \qquad (12)$$

both n, a real positive, and B^* are materials parameters. Substituting (11) into (10) gives

$$\frac{dB}{dx} + \text{signo}(J)\frac{\mu_0 J_{c0}}{\left(1+\frac{B}{B^*}\right)^n} = -\frac{\mu_0 C'}{\rho}.$$

If it is defined that $C' \equiv J_{c0}\rho C$, then

$$\int_{B(x_0)}^{B(x)} \frac{\left(1+\frac{B}{B^*}\right)^n}{C\left(1+\frac{B}{B^*}\right)^n + 1} dB = -\mu_0 J_{c0}(x - x_0),$$

for $x \in [0, D/2]$, and

$$\int_{B(x_0')}^{B(x')} \frac{\left(1+\frac{B}{B^*}\right)^n}{C\left(1+\frac{B}{B^*}\right)^n - 1} dB = -\mu_0 J_{c0}(x' - x_0')$$

for $x' \in [D/2, D]$.

According to the symmetry of the problem and the isotropy of the material, magnetic induction at the face $x = 0$ is the same at the face $x = D$, that is, $\mu_0 H = B(x = 0) = B(x = D)$.

Thus, we can argue that penetration of magnetic induction into the material will occur with the same proportion at both faces, see Scheme 1. This last assertion allow us to write the relations $x' = D - x$ and $B(x) = B(D-x)$. If we choose $x_0 = x_0' = D/2$ and add the last two relations, we find the following:

$$\int_{B(D/2)}^{B(x)} \left\{\frac{\left(1+\frac{B}{B^*}\right)^n}{C\left(1+\frac{B}{B^*}\right)^n + 1} + \frac{\left(1+\frac{B}{B^*}\right)^n}{C\left(1+\frac{B}{B^*}\right)^n - 1}\right\} dB = 0.$$

Since the previous equation follows for each subinterval $[B(D/2), B(x)] \subset [B(D/2), B(D)]$, then, the integrand is equal to zero for $B(x) \in [B(D/2), B(D)]$ and, consequently, the integration constant is found to be $C = 0$. The latter procedure is analogous for magnetic fields H in $-\hat{z}$ direction, obtaining again the integration constant $C = 0$.

Given the symmetry of the system, current density flows in the $+\mathbf{e}_y$ direction in the interval $x = [0, D/2]$, and flows in the $-\mathbf{e}_y$ direction in the interval $x = [D/2, D]$, leading to the following solutions:

$$\left(1+\frac{B}{B^*}\right)^{n+1} = \begin{cases} \left(1+\frac{B(x_0)}{B^*}\right)^{n+1} - \frac{\mu_0 J_{c0}(n+1)}{B^*}(x - x_0) & x \in [0, D/2] \\ \left(1+\frac{B(x_0')}{B^*}\right)^{n+1} + \frac{\mu_0 J_{c0}(n+1)}{B^*}(x - x_0') & x \in [D/2, D] \end{cases} \qquad (13)$$

In general, one can write the above equation considering the two possible incident magnetic field directions, $H > 0$ and $H < 0$, as follows:

$$\left(1+\frac{B}{B^*}\right)^{n+1} = \begin{cases} \left(1+\frac{B(x_0)}{B^*}\right)^{n+1} - \text{sgn}(H)\frac{\mu_0 J_{c0}(n+1)}{B^*}(x - x_0) & x \in [0, D/2] \\ \left(1+\frac{B(x_0')}{B^*}\right)^{n+1} + \text{sgn}(H)\frac{\mu_0 J_{c0}(n+1)}{B^*}(x - x_0') & x \in [D/2, D] \end{cases} \qquad (14)$$

For our purposes, it is convenient to define the quantities $B_{PB} \equiv \mu_0 J_{c0} D/2$ and $b_{><} \equiv 1 + B/B^*$, where the $><$ label refers to the $H > 0$ or $H < 0$ case, respectively. Thus (14) can be written as follows:

$$b_{><}^{n+1}(x) = \begin{cases} b_{><}^{n+1}(x_0) - \text{sgn}(H)\frac{2B_{PB}(n+1)}{DB^*}(x - x_0) & x \in [0, D/2] \\ b_{><}^{n+1}(x_0') + \text{sgn}(H)\frac{2B_{PB}(n+1)}{DB^*}(x - x_0') & x \in [D/2, D] \end{cases} \qquad (15)$$

Therefore, all the solutions for $b_{><}^{n+1}(x)$ are straight lines with the same slope, and opposite sign depending on the interval $x \in [0, D/2]$ or $x \in [D/2, D]$.

3. The characteristic B_P and B_{PP} fields

Without a remanent field, the magnetic induction is gradually distributed as the external magnetic field H is increased. Once the external field reaches the particular value $\mu_0 H_{><} = B_{P><}$, the so-called penetration field, then magnetic induction is completely distributed through the sample. In our notation, this is equivalent to $b_{><}^{n+1}(x = D/2) = 1$.

For $x \in [0, D/2]$, if $x_0 = 0$ and considering the boundary condition, we found that

$$b^{n+1}_{><}(x_0) = b^{n+1}_{a><} = (1 + \mu_0 H_{><}/B^*)^{n+1}.$$

If $|\mu_0 H| < |B_P|$ exists a point $x = x_1$ such that $b^{n+1}_{><}(x_1) = 1$, then

$$x_1 = \text{sgn}(H)\frac{DB^*}{2B_{PB}(n+1)}(b^{n+1}_{a><} - 1).$$

Similarly, for $x \in [D/2, D]$, there is a value $x = x_0' = x_2$ such that $b^{n+1}_{><}(x_0') = 1$ and, at $x = D$, $b^{n+1}_{><}(D) = b^{n+1}_{a><}$, therefore:

$$b^{n+1}_{a><} = 1 + \text{sgn}(H)\frac{2B_{PB}(n+1)}{DB^*}(D - x_2)$$

and

$$x_2 = D - \text{sgn}(H)\frac{DB^*}{2B_{PB}(n+1)}(b^{n+1}_{a><} - 1) = D - x_1.$$

The penetration field $b^{n+1}_{P><}$ can be obtained when $x_1 = x_2 = D/2$:

$$b^{n+1}_{P><} = \text{sgn}(H)\frac{B_{PB}(n+1)}{B^*} \pm 1. \tag{16}$$

It is easy to show that for external fields $|\mu_0 H| > |B_P|$; that is, for $b^{n+1}_{><}(D/2) \neq 1$, the magnetic induction at the center of the sample obeys the following relation:

$$b^{n+1}_{><}(D/2) = b^{n+1}_{a><} - b^{n+1}_{P><} \pm 1.$$

From this relation, one can argue that the particular value $b^{n+1}_{a><} = b^{n+1}_{PP><}$, defined as the double penetration field, and considering that $b^{n+1}_{P><} = b^{n+1}_{><}(D/2)$, it is related to the penetration field as:

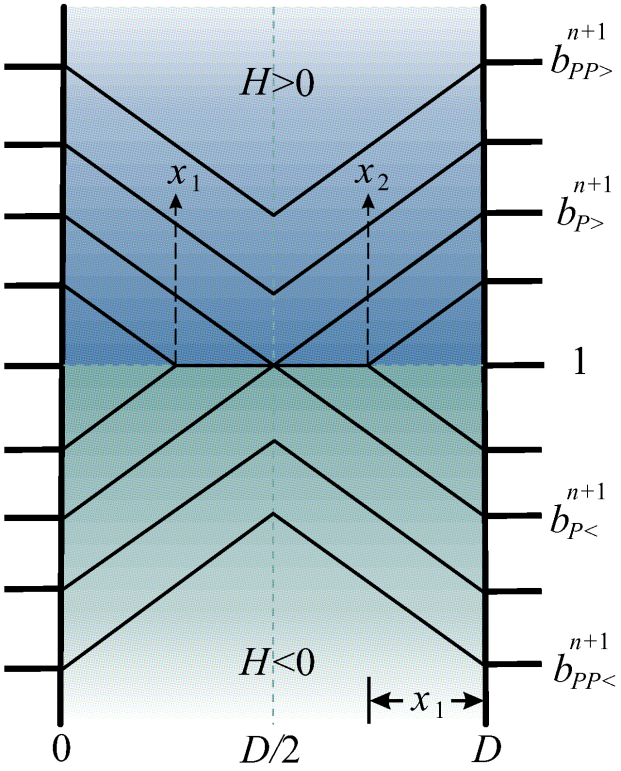

FIGURE 2. Scheme of the $b^{n+1}_{><}(x)$ profiles at a superconducting plate in critical state. Observe the points x_1, x_2, $b^{n+1}_{P><}$ and $b^{n+1}_{PP><}$. The last two points correspond to the cases where the external field reaches the first and second penetration field.

$$b^{n+1}_{PP><} = 2b^{n+1}_{P><} \mp 1. \tag{17}$$

With these results, $b^{n+1}_{><}$ takes the form:

$$b^{n+1}_{><}(x) = \begin{cases} b^{n+1}_{a><} - \text{sgn}(H)\dfrac{2B_{PB}}{DB^*}x & x \in [0, D/2] \\ b^{n+1}_{><}(x_2) + \text{sgn}(H)\dfrac{2B_{PB}}{DB^*}(x - x_2) & x \in [D/2, D] \end{cases} \tag{18}$$

where x_2 defined as:

$$x_2 = \begin{cases} D - x_1 & |B_{a><}| < |B_P| \\ x_1 = D/2 & |B_{a><}| > |B_P| \end{cases}$$

and

$$b^{n+1}_{><}(x_2) = \begin{cases} 1 & x_2 \neq D/2 \\ b^{n+1}_{a><} - b^{n+1}_{P><} + 1 & x_2 = D/2 \end{cases}$$

4. Symmetry relations between $b^{n+1}_{>}$ and $b^{n+1}_{<}$

Let us examine the $b^{n+1}_{><}$ space. Remember that the symbols $>$ and $<$ correspond to the cases $H > 0$ and $H < 0$, respectively.

Observe that for $1 < b_{a>} < b_{P>}$ one has $b^{n+1}_{>}(x = x_1) = 1$, and the straight line $b^{n+1}_{<}$ has one of its ends at the same point x_1. Therefore, the relation between the applied fields is given by $b^{n+1}_{a<} = 2 - b^{n+1}_{a>}$, that is, the applied fields suffer an inversion sign and a translation or, in other words, it suffers a reflection over $b^{n+1}_{><} = 1$.

For applied fields $b_{a>} > b_{P>}$, it is found that $b^{n+1}_{>}(D/2) + b^{n+1}_{<}(D/2) = b^{n+1}_{a>} + b^{n+1}_{a<} = \alpha$.

Specifically, employing the formula for B_P yields $b^{n+1}_{P<} = 2 - b^{n+1}_{P>}$. Therefore, α must be equal to 2, thus $b^{n+1}_{a<} = 2 - b^{n+1}_{a>}$ and $b^{n+1}_{<}(D/2) = 2 - b^{n+1}_{>}(D/2)$.

Finally, adding $b^{n+1}_{<}$ and $b^{n+1}_{>}$ for $x \in [0, D/2]$, one gets $b^{n+1}_{>} + b^{n+1}_{<} = b^{n+1}_{a>} + b^{n+1}_{a<} = 2$, thus, $b^{n+1}_{<} = 2 - b^{n+1}_{>}$. For $x \in [D/2, D]$ it is found that $b^{n+1}_{>} + b^{n+1}_{<} = b^{n+1}_{>}(D/2) + b^{n+1}_{<}(D/2) = 2$, thus, $b^{n+1}_{<} = 2 - b^{n+1}_{>}$.

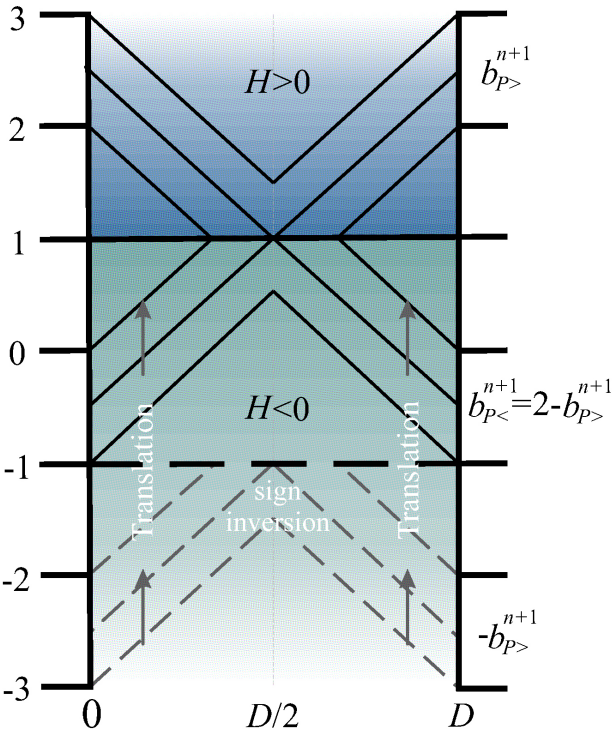

FIGURE 3. Symmetry between $b_{>}^{n+1}$ and $b_{<}^{n+1}$. The magnetic induction curves for $H > 0$ generate the curves $b_{<}^{n+1}$ through a sign inversion plus a translation, given by the formula $b_{<}^{n+1}(x) = 2 - b_{>}^{n+1}(x)$. Under the linear transformation $L\{f(b) + g(b)\} = L\{f(b)\} + L\{g(b)\}$ such that $L\{h(b)\} = (h(b))^{\frac{1}{n+1}}$, one obtains, $b_{<} = 2 - b_{>}$, which preserves the translation and sign inversion.

In conclusion, the magnetic induction curves obtained for $H > 0$ are generators of the $H < 0$ curves, and viceversa, through an inversion sign and translation described by:

$$b_{<}^{n+1}(x) = 2 - b_{>}^{n+1}(x). \tag{19}$$

This reflection mechanism is illustrated in Fig. 3. Notice that when a linear transformation $L\{f(b) + g(b)\} = L\{f(b)\} + L\{g(b)\}$ is applied to Eq. (19), that is, $L\{h(b)\} = (h(b))^{1/(n+1)}$, the result $b_{<} = 2 - b_{>}$ indicates that once $b_{>}$ is known, under an inversion sign and a translation, the $b_{<}$ distribution can be obtained. This result is of particular relevance, since we are dealing with $n-$roots calculation. When magnetic induction takes on negative values, imaginary values for $n-$odd and real values for $n-$even are obtained. In contrast, since $b_{>}$ is strictly greater than zero, one can always find a unique $n-$positive root by employing our proposal.

5. Power and Vertical Law Equivalence

Modelling the $E - J$ relationship for a type-II superconductor, is a subject still under study. Frecuently, the *vertical law* (presented above) or the *power law* $E = E_c(J/J_c)^m$ are used; these approximations give quite good results.

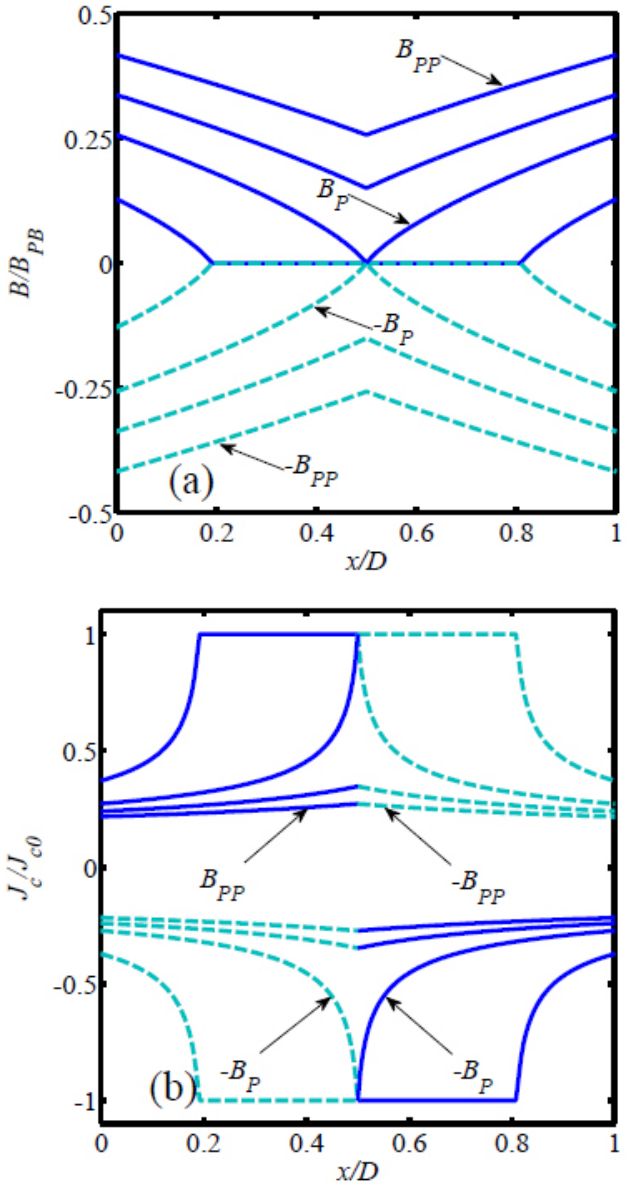

FIGURE 4. (a) B behavior. Continuous lines are the profiles when the applied field has **z** direction, the dashed lines correspond to a external field with $-\mathbf{z}$ direction. (b) The corresponding current density curves of (a). For both graphics, the parameters employed were $B^* = 0.02$ and $n = 0.5$.

The *power law* has proved its effectiveness if one wishes to study the physics of *flux creep*, a response of the thermal energy to both the current driven force and the magnetic flux density gradient. Flux creep is revealed in two ways: 1) it drives slow changes in the magnetic induction and 2) causes measurable resistive voltages.

In classic type-II superconductors, slow flux creep is unobservable unless the flux density gradient reaches its critical value. On the other hand, in HTSC, the magnetic flux movement becomes prominent as flux line bundles are thermally depinned, even at temperatures below T_c. Activation energy $U(J)$ dependence on the current can be extracted from creep

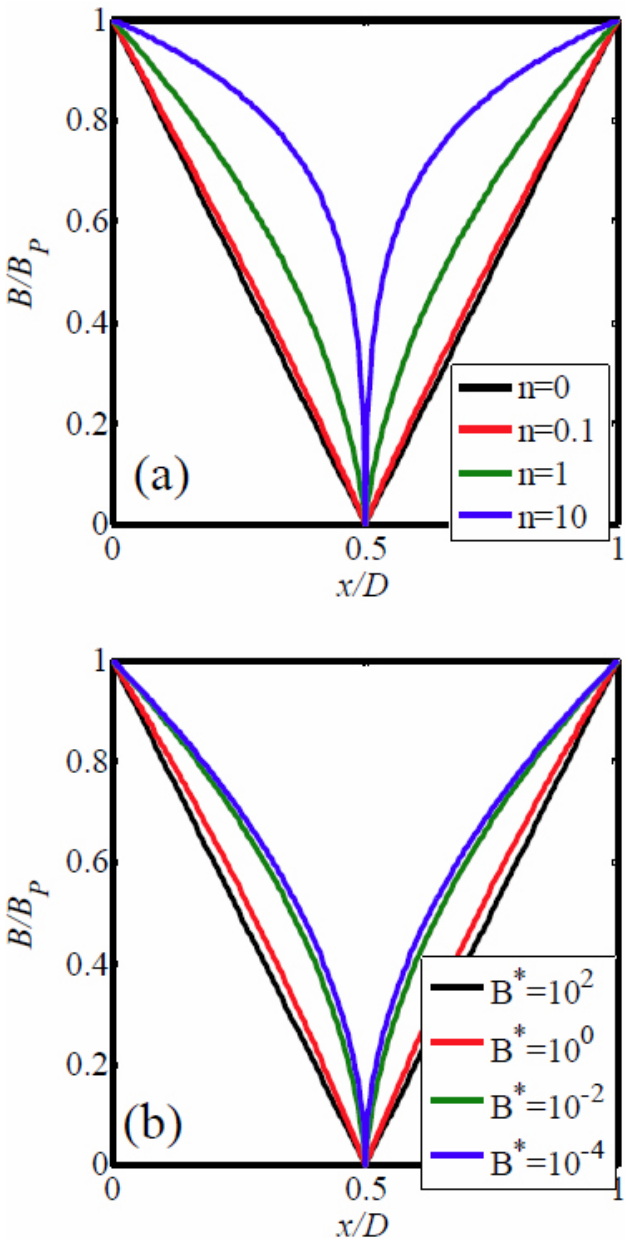

FIGURE 5. Scaled magnetic induction B/B_P vs x/D, for $\mathbf{H} = H\mathbf{e}_z > 0$, varying the parameter n or B^*. (a) $B^* = 0.02$ is fixed; n takes the values $0, 10^{-1}, 1, 10^0$. (b) $n = 1$ is fixed with values $B^* = 10^{-4}, 10^{-2}, 10^0, 10^2$.

measurements, with the power law $E \sim J^m$ being the suggested function to model it [14,15]. Moreover, energy dissipation associated with flux creep can produce catastrophic consequences, originating flux jumps that tend to destroy the critical state [16]. Therefore, the importance of the $E(J)$ choice depends on the type-II superconductor, low or high T_c, and which regime is it in.

Now, substituting the power law in the steady-state equation and calculating its $m-$root, yields:

$$\frac{dB}{dx} = -\mu_0 \text{signo}(J) J_c \left(\frac{C'}{E_c}\right)^{1/m}$$

Denoting $C \equiv (C'/E_c)^{1/m}$ and substituting the current-field relationship (11) in the latter, one can obtain the same solution (14) employing the vertical law if $C \equiv 1$ is chosen. Therefore, in the steady-state approximation, both models describe exactly the same physical environment, making them indistinguishable.

6. Results

Let us apply the theory of the preceding section to obtain the magnetic induction $B(x)$ and current density $J(x)$ profiles as an external field $\mathbf{H} = H\mathbf{e}_z$ parallel to the sample plane varies from 0 to 0.4 T. We consider a model sample with thickness $D = 2.3 \times 10^{-4}$ m, parameters $B^* = 0.02$ T, $n = 0.5$, maximum critical current density $J_c(0) = 4.48 \times 10^9$ Am^{-2}, and $B_{PB} = \mu_0 J_{c0} D/2 = 0.65$ T.

Figure 4 shows the B and J behavior for $H > 0$ (continuous curves) and $H < 0$ (dashed curves). In panel (a) one can observe the magnetic induction profiles when the external field has partially penetrated the superconducting plate, when it reaches the penetration field (labeled B_P), and the double penetration field (labeled B_{PP}). As the applied field is increased, the B profiles tend toward lines with constant slope; the corresponding critical current density, see panel (b), which starts with the maximum critical current value J_{c0}, where the magnetic field has not been penetrated, tends toward constant values along the thickness sample, below J_{c0}.

Figure 5 shows the B profiles when the applied field corresponds to the penetration field $B_{P>}$, varying the parameter n with fixed B^*. Observe, at panel (a), the dimensionless B/B_P critical-state profiles as n is increased one order of magnitude, from zero to 10^0, for a fixed $B^* = 0.02$T. Starting from the Bean case (for $n = 0$), for a poor type-II superconductor (for $n = 10$), where the profile tends toward a uniform field case. On the other hand, Fig. 5(b) shows B/B_P profiles varying the parameter B^* with fixed n. In this case, to appreciate differences between the B/B_P

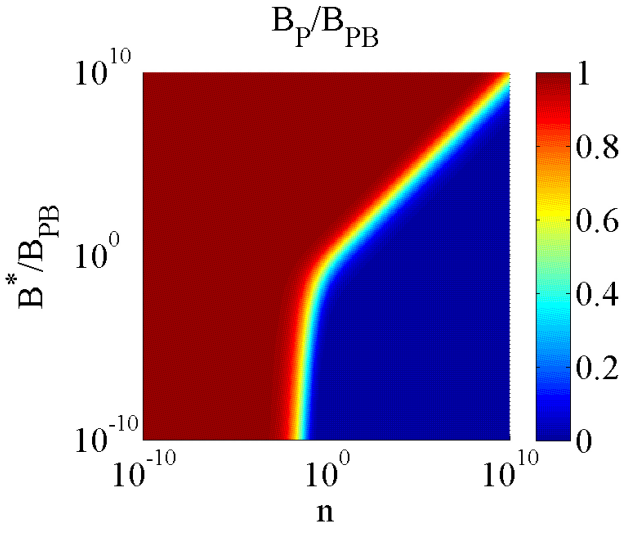

FIGURE 6. Surface plot of dimensionless penetration field B_P/B_{PB} at $x = D/4$.

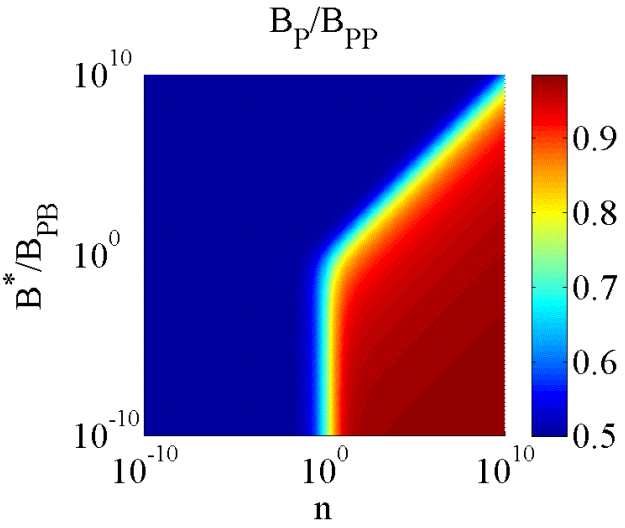

FIGURE 7. Surface plot, at $x = D/4$, of the ratio of the first penetration field, B_P, to the double penetration field, B_{PP}.

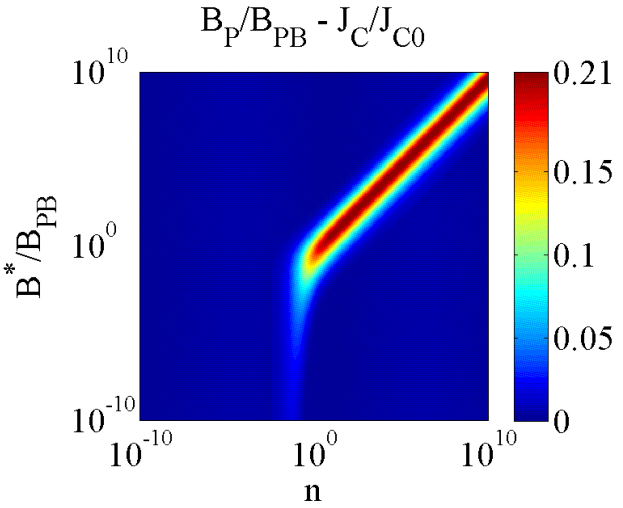

FIGURE 8. Surface plot of dimensionless difference $B_P/B_{PB} - J_c/J_{c0}$ at $x = D/4$.

critical-state profiles, one should select decreasing values of B^* varying it two orders of magnitude from 10^2 to 10^{-4} with fixed $n = 1$. We obtain a Bean profile for B^* large ($B^* = 10^2$T) and, as B^* diminishes, the changing rate of the profiles tending to a poor type-II superconductor case is slower than the case when n varies for a fixed B^*.

As Ming Xu *et. al.* [13] suggested, the material parameters n and B^* may be related to intrinsic and extrinsic properties of the superconductor. In the following section, we study how physical properties are modified as the parameters n and B^* vary. We focus in the case $H > 0$ to obtain the surface plot viewed from above (the so-called *pseudocolor plot* in Matlab) of both dimensionless penetration field B_P/B_{PB} and the double penetration field B_{PP}/B_P, and the difference between the dimensionless penetration field less the dimensionless critical current density, $B_P/B_{PB} - J_c/J_{c0}$, all at $x = D/4$.

In the framework of this theory, the penetration field is obtained as a function of the parameters n, B^*, the intrinsic property J_c, the extrinsic property D and B_{PB}. However, according to the expressions presented in this paper, there is ambiguity in the parameters n and B^* selection because one can find an infinity of values for n and B^* which correspond to a single penetration field value. This is observable in Fig. 6. Theoretically, the maximum value that can be reached is B_{PB}, and, the minimum value is zero; the latter result may be physically inadmisible as the minimum value of the magnetic field is the first critical field, H_{c1}. Let us observe the blue zone, which corresponds to cases close to the limiting Bean case, while the red zone is associated with a poor type-II superconductor, where the critical current density tends to dissapear. The interest zone, where the magnetic induction profiles are not straight lines, is the color gradient. In the graphic there are two regions where the relation between parameters n and B^* is approximately linear. On the other hand, there is a bending at the color gradient zone in the interval $10^{-2} \lessapprox n \lessapprox 1$ and $10^{-4} \lessapprox B^*/B_{PB} \lessapprox 1$.

Since the surface plot for the dimensionless double penetration field has a similar structure to the dimensionless penetration field one, then, to distinguish them, we present the surface plot B_P/B_{PP} in the Fig. 7. Of course, this quotient is less than the unity; the graphic shows a blue zone where $B_{PP} = 2B_P$, which corresponds to superconducting states very similar to those of the Bean case. The red gradient zone suggests us that B_{PP} tends to B_P; this value corresponds to a poor type-II superconductor. Observe that states different than the Bean case or a poor type-II superconductor are better defined at the color gradient zone, where the correlation between the parameters n and B^* is simple, than at the zone obtained for the penetration field. The surface plot of the dimensionless critical current density, that is, the quotient J_c/J_{c0} has also a structure similar to that of the surface plot of B_P/B_{PB}. Therefore, is better to graph the difference $B_P/B_{PB} - J_c/J_{c0}$, presented in Fig. 8. It is evident that the main deviations are generated from $n > 1$ and $B^*/B_{PB} > 1$.

Finally, as an example to show the utility of our results, we present results of a property of the superconducting materials in Fig. 9: the shielding field ability ΔH_{sh}. It is already known that when a magnetic field is applied to a superconductor, and its magnitude is increased by certain ΔH, current density diminishes, the size of the such an increase may produce magnetic instabilities, and consequently, may generate flux jumps. Given the instability criterium, that is, if $\Delta H_{sh} > \Delta H$ the field configuration becomes unstable, ΔH_{sh} can be found by the equation:

$$\Delta H_{sh} = \int_0^{D/2} \Delta J_c dx \tag{20}$$

where ΔJ_c is the change in critical current density associated with an external field H increase from H to $H + \Delta H$.

Figure 9 presents an example of the shielding field ability ΔH_{sh} for $B^* = 1, 10^{-1}, 10^{-2}, 10^{-3}, 10^{-4}$, a fixed $n = 1$,

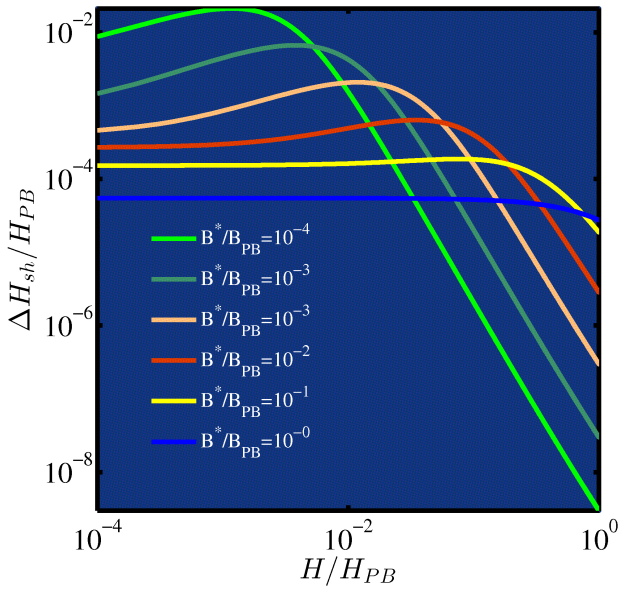

FIGURE 9. Shielding field ΔH_{sh} curves for fixed $n = 1$, $\Delta H/H_{PB}$ varying $B^* = 1, 10^{-1}, 10^{-2}, 10^{-3}, 10^{-4}$.

and $\Delta H/H_{PB} = 10^{-4}$. The orange curve (for $B^* = 1$) represents a stable system for all the external field values.

7. Summary

We have theoretically investigated how the parameters n and B^*, corresponding to the Kim-Anderson generalized function $J_c(B)$, affect the physical characteristics of magnetic induction in a type-II superconductor.

In contrast to previous works, we have obtained a colored map or pseudocolor plot which clearly shows the pair of parameteres n and B^* that describe a range from a Bean-like type-II superconductor to a poor one. Between these limiting cases, we found a rich area with a color gradient corresponding to equivalent states. Therefore, ambiguity persists regarding the choise of values for n and B^*.

We consider that additional theoretical studies are needed. Specifically within this framework, the hysteresis curve could contribute to a better understanding of the physical meaning of the n and B^* parameter pair.

Acknowledgments

This research was supported by: (C. Romero-Salazar) PROMEP/103.5/10/4975 and (O.A. Hernández-Flores) SEP-CONACYT-CB-2008-01-106433.

1. C.P. Bean, *Phys. Rev. Lett.* **8** (1962) 250.
2. John. R. Clem and Antonio Perez-Gonzalez, *Phys. Rev. B* **30** (1984) 5041.
3. Antonio Perez-Gonzalez and John. R. Clem, *J. Appl. Phys.* **58** (1985) 4326.
4. A. Badía y C. López, *Phys. Rev. Lett.* **87** (2001) 127004.
5. I.F. Voloshin, A.V. Kalinov, S.E. Savel'ev, L.M. Fisher, V.A. Yampolskiĭ, and F. Perez Rodriguez, *JETP* **84** (1997) 1063.
6. S.E. Savel'ev, L.M. Fisher, V.A. Yampolskiĭ *JETP* **85** (1997) 1063.
7. C. Romero-Salazar and F. Pérez-Rodríguez, *Appl. Phys. Lett.* **83** (2003) 5256.
8. J.R. Clem, *Phys. Rev. B* **83** (2011) 214511 .
9. D.-X. Chen and R. B. Goldfarb, *J. Appl. Phys.* **66** (1989) 2489.
10. T. H. Johansen and H. Bratsberg, *J. Appl. Phys.* **77** (1995) 3945.
11. Z. Kozioł, J. J. M. Franse, P. F. de Châtel, and A. A. Menovsky, *Phys. Rev. B* **50** (1994) 15978.
12. C. Romero-Salazar and F. Pérez-Rodríguez, *Supercond. Sci. Technol.* **16** (2003) 1273.
13. Ming Xu, Donglu Shi, and Ronald F. Fox, *Phys. Rev. B* **42** (1990) 10773.
14. M. Tinkham, *Introduction to Superconductivity* (USA: McGraw-Hill, 1996). p. 148-187.
15. Ernst Helmut Brandt, *Rep. Prog. Phys.* **58** (1995) 1465.
16. C. Romero-Salazar, F. Morales, R. Escudero, A. Durán and O.A. Hernández-Flores *Phys. Rev. B* **76** 104521 (2007).
17. C. Romero-Salazar and F. Pérez-Rodríguez, *Physica C* **404** (2004) 317-321.
18. C. Romero-Salazar, L.D. Valenzuela-Alacio, A.F. Carballo-Sánchez, and F. Pérez-Rodríguez, *J. Low Temp. Phys.* **139** (2005).